Journal of Power Sources 222 (2013) 333–339

Contents lists available at SciVerse ScienceDirect

Journal of Power Sources

journal homepage: www.elsevier.com/locate/jpowsour

Short communication

Improved long-term durability of a parallel-type dye-sensitized solar cell module using a platinum metal grid fabricated by direct current magnetron sputtering with heat treatment

Min-Kyu Son [a], Hyunwoong Seo [b,c], Soo-Kyoung Kim [a], Na-Yeong Hong [a], Byung-Man Kim [a], Songyi Park [a], Kandasamy Prabakar [a], Hee-Je Kim [a,*]

[a] Department of Electrical Engineering, Pusan National University, San 30, Jangjeon-Dong, Geumjeong-Gu, Busan 609-735, Republic of Korea
[b] Graduate School of Information Science and Electrical Engineering, Kyushu University, 744 Motooka, Nishi-ku, Fukuoka 819-0395, Japan
[c] Center of Plasma Nano-interface Engineering, Kyushu University, 744 Motooka, Nishi-ku, Fukuoka 819-0395, Japan

HIGHLIGHTS

- ► Fabrication of dye-sensitized solar cell (DSSC) Pt metal grid current collector by DC magnetron sputtering with heat treatment.
- ► The sheet resistance of the Pt grid is reduced with increasing thickness.
- ► Heat treatment during sputtering is helpful in improving the effect of Pt grid.
- ► The Pt metal grid is more durable than Ag, maintaining 4.1% air mass (AM) 1.5 efficiency after 1700 h.

ARTICLE INFO

Article history:
Received 25 June 2012
Received in revised form
27 August 2012
Accepted 29 August 2012
Available online 6 September 2012

Keywords:
Dye-sensitized solar cell
Parallel-grid module
Platinum metal grid
Direct current magnetron sputtering
Long-term durability

ABSTRACT

A parallel-type grid module is used widely in the dye-sensitized solar cells (DSSCs). In most parallel-grid DSSC modules, silver (Ag) is used as the grid metal owing to its high conductivity. On the other hand, Ag is disadvantageous to the durability of the module because it readily undergoes corrosion from the iodide electrolyte that causes electrolyte degradation. In this study, a Ag grid in a parallel DSSC module is replaced by a platinum (Pt) grid to improve the stability of the parallel DSSC module. The Pt grid is fabricated by direct current magnetron sputtering with substrate heat treatment. Although the sheet resistance of the Pt grid is slightly higher than that of the Ag grid, the Pt grid is effective as a grid structure, reducing the internal series resistance in the DSSC. Furthermore, the durability of the Pt grid module is improved, maintaining 4.1% air mass (AM) 1.5 efficiency after 1700 h, because no electrolyte degradation or corrosion of the grid structure occurs.

1. Introduction

Dye-sensitized solar cells (DSSCs) have attracted considerable attention as an alternative to conventional silicon solar cells due to their low manufacturing cost, simple fabrication process, flexibility, and transparency [1,2]. Accordingly, considerable attempts have been made to apply DSSCs to a range of real-life applications, such as building-integrated photovoltaics (BIPV) and electronics-integrated photovoltaics (EIPV) [3]. In these applications, the efficiency and durability of DSSCs are significant because they need to provide long-life electric power. In recent years, ongoing intensive studies have made the efficiency competitive with those of other photovoltaic cells. As a result, maximum efficiencies of 12.3% in a single cell and 9.9% in a submodule have been recorded [4,5]. On the other hand, the durability of DSSCs is insufficient for commercial applications for several reasons, such as leakage of the liquid electrolyte and degradation of the components. This is still a challenging problem that has impeded the commercialization of DSSCs despite the development of a solid electrolyte [6–8] and the extensive studies on substantial sealant materials [9–11] and robust compositions [12–14] to improve their durability.

Module structures have been adopted for DSSCs, as for other commercial photovoltaics. A range of module structures have been suggested, such as the Z-type module [10], W-type module [15,16],

* Corresponding author. Tel.: +82 51 510 2364; fax: +82 51 513 0212.
E-mail address: heeje@pusan.ac.kr (H.-J. Kim).

0378-7753/$ – see front matter © 2012 Elsevier B.V. All rights reserved.
http://dx.doi.org/10.1016/j.jpowsour.2012.08.080

monolithically series-interconnected module [17,18] and parallel-connected module [19–21]. The first three type modules are called series-connected modules because single cells are connected in series to obtain a high output voltage. On the other hand, in a parallel-connected module, single cells are connected in parallel, resulting in a high output current. In this module structure, a metal grid structure is essential for high efficiency, unlike a series module structure. This structure, which has relative low resistance, provides an effective pathway to move electrons without loss from the module to an external load. Therefore, a high output current can be obtained in a metal grid parallel-connected module.

The metals evaluated for a grid structure include silver (Ag), nickel (Ni), copper (Cu) and aluminium (Al) [22,23]. Among these, Ag is widely used as a grid metal because of its high electrical conductivity. However, these metals (including Ag) are corroded easily by the liquid electrolyte, which consists of the iodide/triiodide redox couple [23,24]. This causes instability of DSSCs, along with thermal deterioration [25], degradation by humidity [11] and leakage of the liquid electrolyte [26]. Therefore, absolute protection of the metal grid is essential to avoid corrosion of the grid by the electrolyte, resulting in improved stability. In general, a robust glass frit and heat-resistant polymer are used to prevent corrosion between the electrolyte and metal grid. These protection methods, however, have limitations in inhibiting this corrosion reaction over a long period because continuous irradiation of sunlight and the humid environment weaken the grid protection structure. Therefore, exposure of the grid structure to the electrolyte is likely to be increased further, which will accelerate the corrosion reaction between the grid and electrolyte as well as electrolyte degradation, resulting in a deterioration of the DSSC module performance.

A metal that can resist corrosion from the electrolyte is a potential replacement for corrosion-prone metal grids, particularly Ag. Such a metal will act as a current collecting grid and prevent electrolyte degradation, despite being exposed to the electrolyte. Platinum (Pt) has good conductivity and is almost invulnerable to corrosion by the electrolyte. Therefore, platinum will be suitable for a non-corroding metal grid. Although the Pt is expensive than the Ag in point of the raw materials [27], the cost of metal grid is a small proportion of the total DSSC production cost [28]. In addition, the maintenance cost, which is around 40% in the total DSSC production cost [28], can be reduced by enhancing the long-term stability of the DSSC module because of the non-corroding Pt grid. Overall, the usage of the Pt metal grid in the DSSC module is advantageous to not only the improvement of the long-term stability of the DSSC but also the reduction of the total DSSC production cost. In this paper, a parallel-connected module with a Pt grid, which was fabricated by direct current (DC) magnetron sputtering, was examined to improve the durability of DSSCs. The performance of the Pt grid was enhanced by using the optimal fabrication parameters and the effect of the Pt grid as a current collecting grid was demonstrated by analyzing the performance of a single cell in a parallel-connected module. And the grid exposure test to the electrolyte was conducted to compare the corrosive reactions with the iodine electrolyte between Ag and Pt. Finally, a long-term stability test was conducted to confirm the durability of the Pt grid module, compared to the conventional Ag grid module.

2. Experiments

Iodine (I_2), lithium iodide (LiI), 4-tertbutylpyridine, and acetonitrile were purchased from Sigma–Aldrich (Saint Louis, USA). Acetone and ethanol were used as provided from Samchun Pure Chemical Co. LTD (Pyeongtaek, Korea). And N719 dye (cis-bis(isothiocyanato) bis(2,2′-bipyridyl-4,4′-discarboxylato)–ruthenium(II)–bis tertabutyl–ammonium, $RuC_{58}H_{86}N_8O_8S_2$) powder was the commercial product obtained from Solaronix (Aubonne, Switzerland).

A fluorine-doped tin oxide (FTO, 13 Ω square^{-1}, Hartford Glass Co. Inc, Hartford City, USA) substrate for a 2.4 cm^2 active area cell was prepared by sequential ultrasonic rinses with acetone, ethanol and distilled water for 10 min, followed by dry-cleaning with a nitrogen stream. A Pt grid was deposited on a cleaned FTO substrate by DC magnetron sputtering at a power of 150 W and a working pressure 333.3 mPa with argon (Ar) gas. The thickness of the Pt grid was controlled by the deposition time. The FTO substrate was heated to 150 °C during the sputtering process to strengthen the performance of the grid. For Ag grid fabrication, a Ag paste (590-G, Electro-Science Laboratories Inc., King of Prussia, USA) was deposited on a cleaned FTO by screen printing. This was completed by an additional dry process at 125 °C for 10 min followed by sintering at 450 °C for 30 min.

The prepared Ag grid was characterized with field emission scanning electron microscope (FE-SEM, Hitachi-S4800, Tokyo, Japan) operated at 15 kV, high resolution transmission electron microscopy (HRTEM, JEM 2011, JEOL Corporation, Tokyo, Japan) with charge coupled device camera (Ultra Scan 400SP, Gatan Corporation, Pleasanton, USA) and X-ray diffraction (XRD, X'pert PRO MRD, PANalytical, Almelo, Netherlands) under optimized operating conditions of 30 mA and 40 kV. The Ag grid consists of spherical Ag nanoparticles having size in the range of 25–50 nm, as shown in the HRTEM image (Fig. 1(b)). And these Ag nanoparticles are strongly combined each other, because the contact between Ag nanoparticles is improved by high sintering temperature, as shown in the SEM image (Fig. 1(a)). Fig. 1(c) shows XRD patterns of the Ag grid. The diffraction peaks at 38.16°, 44.34°, 64.5°, and 77.46° correspond to the (1 1 1), (2 0 0), (2 2 0) and (3 1 1) planes. These correspond to FCC structure of the metallic Ag, according to the JCPDS file 87-0720 [29,30]. This confirms that the prepared Ag grid is well crystallized without oxide impurities. With these results, it is concluded that the prepared Ag grid can provide an effective electron pathway in the DSSC by the dense metal Ag structure. The thicknesses of the Pt and Ag grids were measured using a surface profiler (ET 4000, Dong-Il Techno Co. Ltd., Seoul, Korea), and their sheet resistances were characterized using a 4-point probe meter (FPP-RS8-1G, Dasol ENG., Cheongju, Korea).

To fabricate the photo-electrodes, a titanium oxide (TiO_2) paste (Ti-Nanoxide HT/SP, Solaronix, Aubonne, Switzerland), consisting of 9 nm anatase particles, was deposited on the FTO with the grid structures using the doctor blade method. The TiO_2 deposited photo-electrodes were sintered at 450 °C for 30 min to form a nanoporous structure. The thickness of the sintered TiO_2 nanoporous structure was approximately 15 μm. The resulting photo-electrodes were soaked in a 0.2 mM N719 dye solution for 24 h at room temperature to attach the dye molecules to the photo-electrode. The Pt catalytic layer for the redox process on the counter-electrode was fabricated by depositing a commercial Pt paste (Platisol T/SP, Solaronix, Aubonne, Switzerland), containing a chemical Pt precursor, on the cleaned FTO using the doctor blade method. The platinized counter-electrodes were completed by sintering at 450 °C for 10 min. The prepared photo-electrode and counter-electrode were assembled using thermoplastic hot-melt sealing sheets (SX 1170-60, Solaronix, Aubonne, Switzerland), 60 μm in thickness. Subsequently, a redox electrolyte consisting of 0.5 M LiI, 0.05 M I_2 and 0.5 M 4-tertbutylpyridine in acetonitrile was injected through a pre-drilled hole on the counter-electrode. A module was fabricated in the same way as above.

In this experiment, the single cell was designed as a rectangle type, and the module was composed of 5 rectangular single cells in

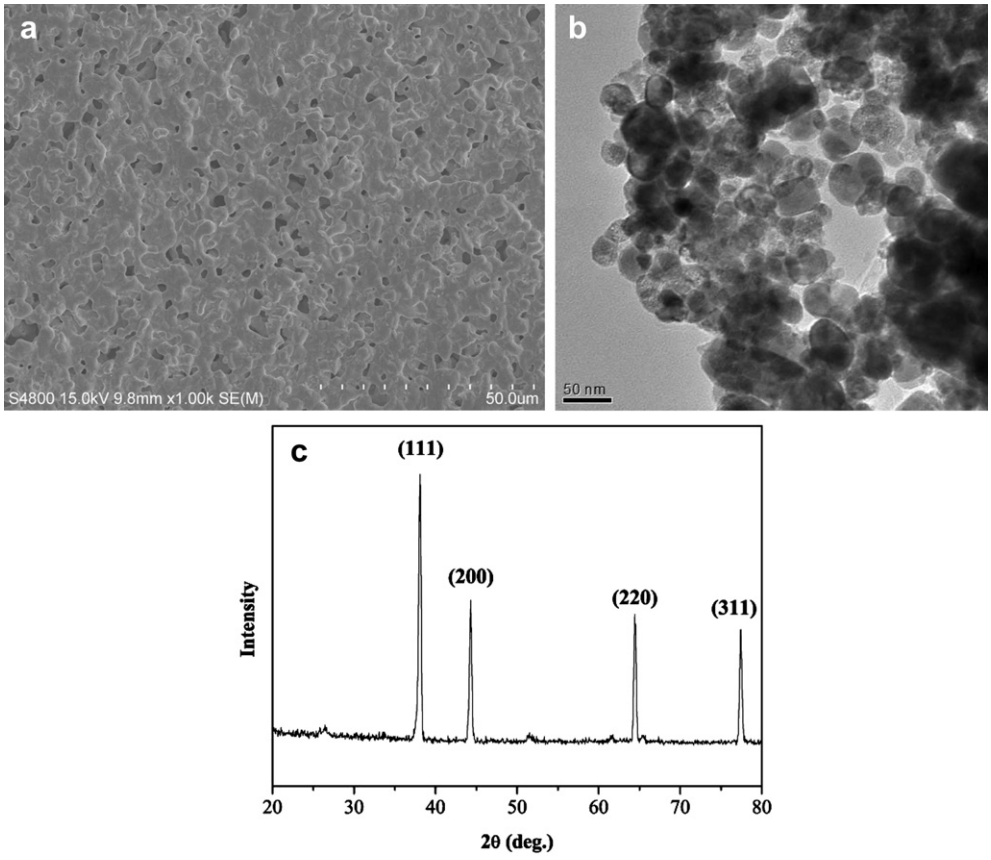

Fig. 1. Morphological characteristics of prepared Ag grid: (a) SEM image (b) HRTEM image and (c) XRD patterns.

a parallel connection. The photovoltaic performance was measured under 1 sun (air mass (AM) 1.5, 100 mW cm^{-2}) using a source meter (Model 2400, Keithley Instrument Inc., Cleveland, USA). The active area was fixed at 2.4 cm^2 in the single cell and at 12.0 cm^2 in the module. During the measurement, the cells and modules were covered with a black mask except for the active area. The *I–V* characteristics examined were the open circuit voltage (V_{OC}), short circuit current (I_{SC}), fill factor (*FF*) and conversion efficiency (η). The internal impedance of the single cells was characterized by electrochemical impedance spectroscopy (EIS, SP-150, BioLogic Science Instruments, Grenoble, France) to examine the effect of the grid. The EIS spectra of the Nyquist diagram were measured over the frequency range from 10 mHz to 1 MHz at room temperature. The applied bias voltage and AC amplitude were set to the V_{OC} of a single cell and 10 mV, respectively. The incident photon to current conversion efficiency (*IPCE*) of the single cells was measured as a function of wavelength from 400 nm to 900 nm under monochromatic irradiation, emitted from a xenon lamp (MAX-302, Asahi Spectra Co. Ltd., Tokyo, Japan) to analyze performances of the single cells. For the long-term stability test, the fabricated modules were exposed to light continuously at room temperature (25 °C) without humidity and their photovoltaic performance was recorded.

3. Results and discussion

Table 1 summarizes the sheet resistance of the Pt grid at different deposition times and substrate heat treatments. As shown in Table 1, the sheet resistance (R_S) of the Pt grid decreases with increasing deposition time, resulting in an increase in grid thickness. Generally, the metal grid resistance (R) is related to the width, length and height of the grid, as shown in Fig. 2, and can be expressed as Eq. (1).

$$R = (\rho \cdot l)/(w \cdot h) \quad (1)$$

where ρ is the resistivity of the metal grid, and w, l and h is the respective width, length, and height of the metal grid [31]. In this experiment, this is only related to the height of the Pt grid, namely the thickness of the Pt grid, because the width and length are fixed to 1.0 mm and 50.0 mm, respectively. The thickness increases at a rate of 250 nm min^{-1} by normal sputtering and at a rate of 310 nm min^{-1} by sputtering with substrate heat treatment. Therefore, R_S of the Pt grid decreases with increasing h because they are inversely proportional to each other, as shown in Fig. 3. Moreover, despite the same deposition time, R_S is reduced further when the substrate is heated to 150 °C during the sputtering process. This is caused by a change in the sputtering environment with heat. More Pt atoms are deposited on the substrate because Ar

Table 1
Sheet resistance (R_S) of the Pt grid after different deposition times and substrate heat treatment.

Deposition time (min)	Normal sputtering		Sputtering with the substrate heat treatment	
	Thickness (nm)	R_S ($\Omega \cdot square^{-1}$)	Thickness (nm)	R_S ($\Omega \cdot square^{-1}$)
1	46.63	57.53	52.46	45.36
5	257.91	3.97	304.54	3.41
10	482.31	2.65	612.00	1.73
15	763.54	1.43	926.74	1.09

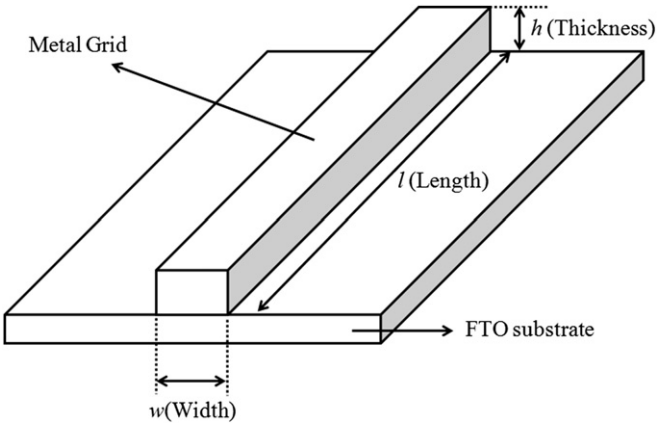

Fig. 2. Schematic diagram of the grid structure in a parallel-grid DSSC module.

ions in plasma are accelerated more by increasing the temperature in the sputtering atmosphere. This is helpful for increasing the thickness of the Pt grid, resulting in a decrease in R_S, as well as for improving contact between the grid and substrate.

As shown in Table 1 and Fig. 3, R_S of the Pt grid becomes saturated at approximately 1 Ω square^{-1}. This value is higher than that of the Ag grid (0.059 Ω square^{-1}). The thickness of the Pt grid fabricated by sputtering with substrate heat treatment for 15 min (926.74 nm) is one-tenth of the thickness of the conventional Ag grid (10 μm). In addition, the inherent ρ values are different: 1.59×10^{-8} Ω m and 1.06×10^{-7} Ω m in the case of the Ag and Pt, respectively [32]. These can explain the difference in R_S between the Pt and Ag grid. Although it is possible to decrease R_S of the Pt grid by increasing the thickness, there is a limitation because some cracks are formed in the Pt grid with a deposition time >15 min. Therefore, sputter deposition with a substrate heat treatment for 15 min is used as the fabrication conditions of the Pt grid. The Pt metal grid fabricated under this condition is suitable as a current collecting grid despite its higher R_S, than that of Ag because R_S (1.092 Ω square^{-1}) is much lower than that of bare FTO.

The performance of the single cells is listed in Table 2, and the *I–V* characteristic curves of the single cells with no grid (No-grid cell), Pt grid (Pt-grid cell) and Ag grid (Ag-grid cell) are shown in Fig. 4.

Table 2
Performance of the single cells: No-grid cell, Pt-grid cell, and Ag-grid cell.

Single cells	V_{OC} (V)	I_{SC} (mA)	*FF*	η (%)
No-grid cell	0.62	29.05	0.48	3.63
Pt-grid cell	0.61	27.16	0.65	4.51
Ag-grid cell	0.61	26.44	0.72	4.87

The η value of a single cell with the Pt grid is superior to that without the grid structure but is slightly lower than that with the Ag grid because the R_S of the Pt grid is slightly higher than that of the Ag grid, as mentioned previously. This is caused mainly by the increase in *FF*, which is related to the internal resistance of the DSSC. An improvement in *FF* means that electron transport in the DSSC is enhanced by reducing R_S, which is one of the internal resistances. This suggests that the Pt grid is effective in reducing the internal resistance as a current collecting grid. This is also confirmed by the internal impedances analysis from the EIS Nyquist diagram.

Fig. 5 presents the internal impedance spectra of the single cells: No-grid cell, Pt-grid cell and Ag-grid cell. The internal impedance components in the DSSC are generally expressed as the frequency-independent impedance (R_0) and three semi-circles in the Nyquist diagram. These semi-circles are attributed to the redox reaction at the counter-electrode in the high frequency range, electron transfer at the TiO_2/dye/electrolyte interface in the middle frequency range, and charge transport by ions within the electrolyte in the low frequency range, which is barely observable in Fig. 5 [33]. The component of R_0, which is shown as the magnitude from the zero point to the start point of the first semi-circle in Fig. 5, is the series resistance including the sheet resistance of conducting glass and the contact resistance of the cell in the transmission line model of the DSSC [34–36]. These values are 27.64 Ω, 4.35 Ω and 1.28 Ω in the No-grid cell, Pt-grid cell, and Ag-grid cell, respectively. The small R_0 in the Pt-grid cell compared to the No-grid cell means that the internal series resistance of the single cell is reduced because the Pt grid with a low R_S produces an effective electron pathway from the TiO_2 nanoporous structure to the external circuit. This results in a higher *FF* in the Pt-grid cell, compared to the single cell without a grid.

While the *FF* increases with the grid structure, the I_{SC} of three single cells is similar, as shown in Table 2. This means that the main

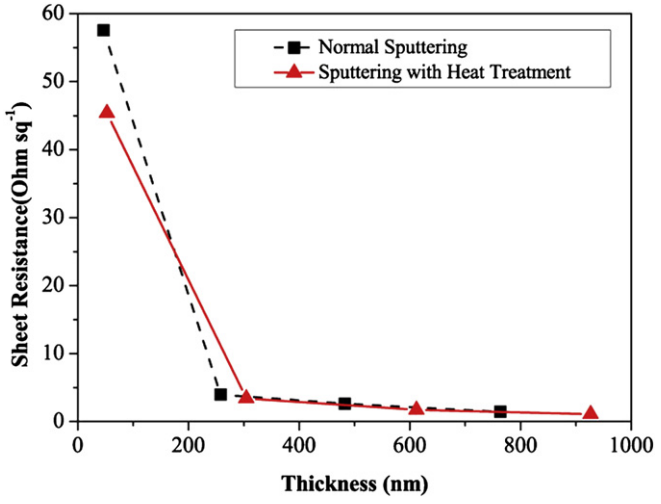

Fig. 3. Relationship between the thickness and sheet resistance (R_S) of the grid when the grid was fabricated by normal sputtering (dotted line with square points) and sputtering with substrate heat treatment (solid line with triangle points).

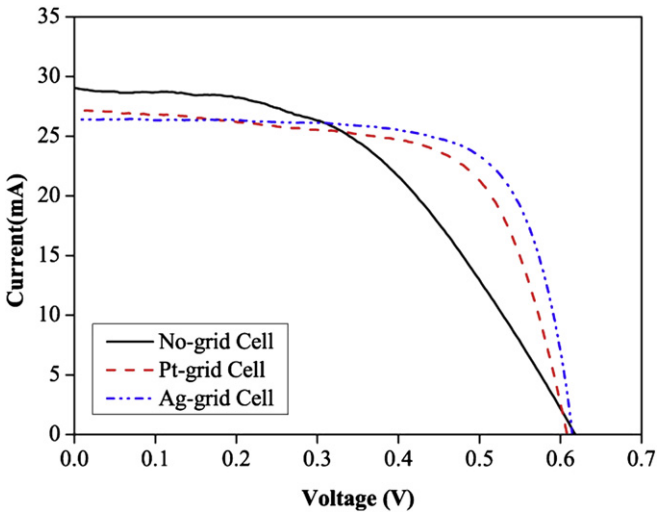

Fig. 4. *I–V* characteristic curves of the single cells with no grid (No-grid cell, solid line), Pt grid (Pt-grid cell, dotted line) and Ag grid (Ag-grid cell, double-dotted line).

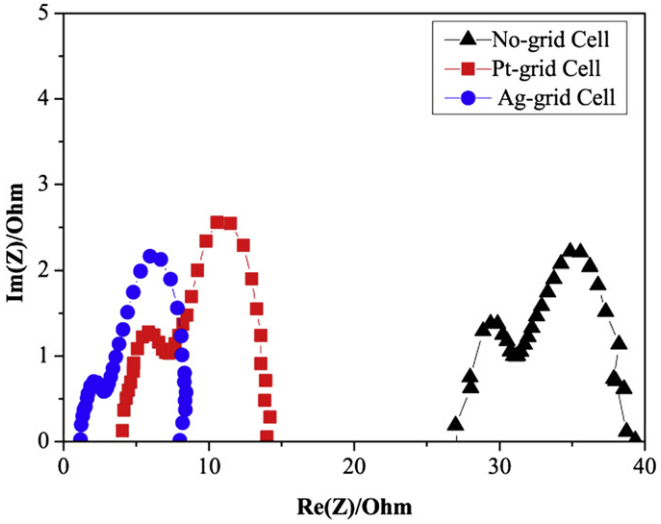

Fig. 5. Internal impedance spectra of the single cells: No-grid cell (triangle points), Pt-grid cell (square points) and Ag-grid cell (circle points).

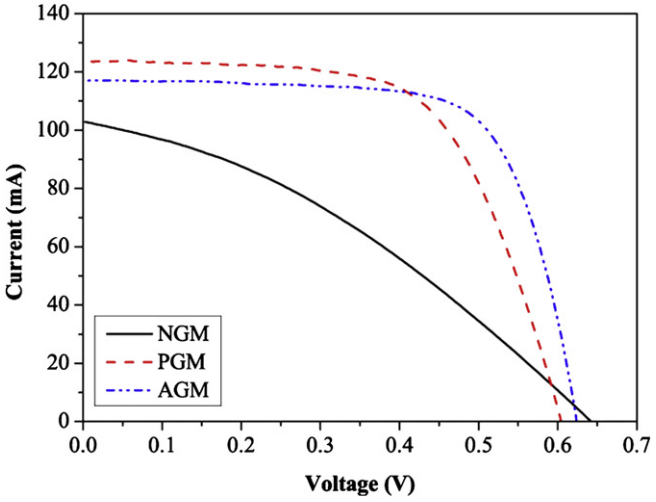

Fig. 7. Initial performance of the fabricated three parallel modules: module without grid (NGM, solid line), module with a Pt grid (PGM, dotted line), and module with a Ag grid (AGM, double-dotted line).

role of grid structure is to improve the electron transport in the DSSC, not to generate more electrons. This fact is demonstrated by *IPCE* spectra of three single cells: No-grid cell, Pt-grid cell and Ag-grid cell, as shown in Fig. 6. In the DSSCs, the current density (J_{SC}) is expressed as Eq. (2).

$$J_{SC} = \int qF(\lambda)(1 - r(\lambda))IPCE(\lambda)\mathrm{d}\lambda \quad (2)$$

where q is the electron charge, $F(\lambda)$ is the incident photon flux density at wavelength λ, $r(\lambda)$ is the incident light loss due to the light absorption and reflection by conducting glass. And the *IPCE* is determined by Eq. (3).

$$IPCE(\lambda) = LHE(\lambda)\phi_{e-inj}(\lambda)\eta_{CC}(\lambda) \quad (3)$$

where $LHE(\lambda)$ is light harvesting efficiency, $\Phi_{e\text{-}inj}(\lambda)$ is the electron injection yield from the dye excited state into the TiO_2, $\eta_{CC}(\lambda)$ is the charge collection efficiency at transparent conductive oxide electrodes [33]. The *IPCE* is mainly controlled by the light harvesting efficiency, because the product of $\Phi_{e\text{-}inj}(\lambda)$ and $\eta_{CC}(\lambda)$ is almost 1 [37,38]. And the light harvesting efficiency is determined by the characteristics of dye and capture ability of the irradiated light on the photo-electrode. As shown in Fig. 6, the *IPCE* spectra of three single cells are almost same. This indicates that the light harvesting efficiency of three single cells is similar, because the N719 dye attached TiO_2 photo-electrodes in three single cells are fabricated with same conditions and methods. The grid effect is not shown here, because the grid structure cannot affect the light harvesting efficiency in the DSSC. Therefore, it is concluded that the performance of the DSSC with the Pt grid is improved because of the enhancement of electron transport by the Pt grid, not any other factors.

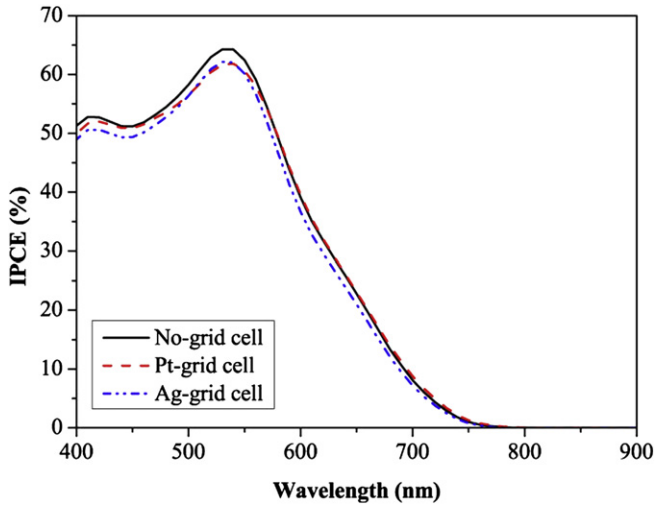

Fig. 6. *IPCE* spectra of three single cells: No-grid cell (solid line), Pt-grid cell (dotted line) and Ag-grid cell (double-dotted line).

The initial performance of the three parallel modules fabricated is shown in Fig. 7: a module without a grid (No Grid Module, NGM), a module with a Pt grid (Pt Grid Module, PGM), and a module with an Ag grid (Ag Grid Module, AGM). A low η is observed in the NGM because of the low *FF* caused by the absence of a grid structure. On the other hand, the η values of the PGM and AGM are higher because of the higher *FF*s than the NGM. This suggests that the Pt grid can improve electron transport, providing an effective electron pathway in a large-scaled DSSC module to prevent electron recombination between the FTO and electrolyte. On the other hand, the initial performance of the PGM is slightly lower than that of the AGM because the performance of Pt as an electron-collecting grid is inferior to that of Ag because of the difference in R_S.

A grid exposure test to the electrolyte is conducted to confirm the inertness of the Pt grid to the electrolyte, compared to the Ag grid. This test is conducted by using single cells with the Ag and Pt

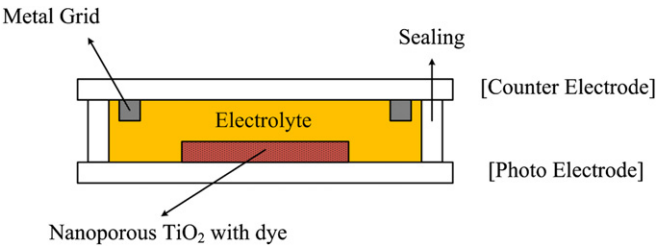

Fig. 8. Schematic diagrams of the grid exposure test.

Table 3
Performance of the DSSCs after grid exposure test to the electrolyte: after 0 h and 24 h.

		V_{OC} (V)	I_{SC} (mA)	*FF*	η (%)
0 h	Pt grid	0.65	20.54	0.43	2.37
	Ag grid	0.16	12.60	0.25	0.21
24 h	Pt grid	0.63	17.06	0.52	2.34
	Ag grid	0.11	9.05	0.26	0.11

Table 4
Comparison of the initial performance and performance after the long-term stability test for 1700 h of the NGM, PGM and AGM.

		V_{OC} (V)	I_{SC} (mA)	*FF*	η (%)
Initial performance	PGM	0.60 ± 0.01	123.99 ± 0.20	0.63 ± 0.02	3.91 ± 0.20
	AGM	0.62 ± 0.02	117.11 ± 0.15	0.71 ± 0.01	4.30 ± 0.17
Performance after 1700 h	PGM	0.63 ± 0.01	119.85 ± 0.15	0.64 ± 0.01	4.03 ± 0.15
	AGM	0.58 ± 0.01	89.15 ± 0.10	0.74 ± 0.02	3.19 ± 0.13

grid on the counter-electrode. As shown in Fig. 8, Ag and Pt grid without the protection structure are exposed directly to the electrolyte to simulate the exposure of the grid structure to the electrolyte, resulting from the weak grid protection structure in the DSSC module. Direct exposure of grid to the electrolyte causes fast reaction with the electrolyte and grid. Therefore, it is easily possible to confirm the change of the grid structure due to electrolyte and the influence of this on the performance of the DSSC. Table 3 lists the performance of the DSSCs, which are measured immediately and 24 h after grid exposure to the electrolyte. As shown in Table 3, the performance of the DSSC without protection for Ag grid deteriorates immediately when the electrolyte reaches the grid. At the same time, the brownish color of the electrolyte turns to colorless. This means that the degradation of the electrolyte occurs by a reaction between the Ag grid and electrolyte. The redox potential of the electrolyte is changed by the degradation of the electrolyte, resulting in a low V_{OC}. Damage to the grid by the electrolyte is also observed after 24 h. In contrast, the performance of the DSSC with Pt grid does not deteriorate despite exposure to the electrolyte for 24 h. This confirms that the Pt grid is inert to corrosion with the electrolyte, whereas the Ag grid is quite sensitive. This shows that a Pt grid is effective in improving the durability of the DSSC modules.

The performance of the NGM, PGM and AGM during the long-term stability test at 25 °C without humidity is recorded in Fig. 9. The performance of all modules is maintained at the initial value until approximately 1000 h. After 1000 h, the performance of the AGM begins to decrease, whereas those of the NGM and PGM are largely maintained. After the long-term stability test for 1700 h, the performance of the AGM is <80% of the initial performance, in contrast to the PGM, whose performance remained essentially constant. The main reasons for this deterioration are the decreases in V_{OC} and I_{SC}, as listed in Table 4. These are caused by electrolyte degradation and corrosion of the Ag grid. The former changes the redox potential of the electrolyte, resulting in a low V_{OC}. The latter interrupts the effective and rapid electron transport to the external circuit, resulting in a low I_{SC}. On the other hand, there is no electrolyte degradation or corrosion of the grid structure in the PGM because the Pt metal is inert to the electrolyte. As a result, the durability of the PGM is improved by maintaining 4.1% AM 1.5 efficiency after 1700 h, compared to that of the AGM, despite the initial performance of the PGM being slightly lower than that of the AGM. Overall, Pt is beneficial for maintaining the role of the grid and preventing electrolyte degradation.

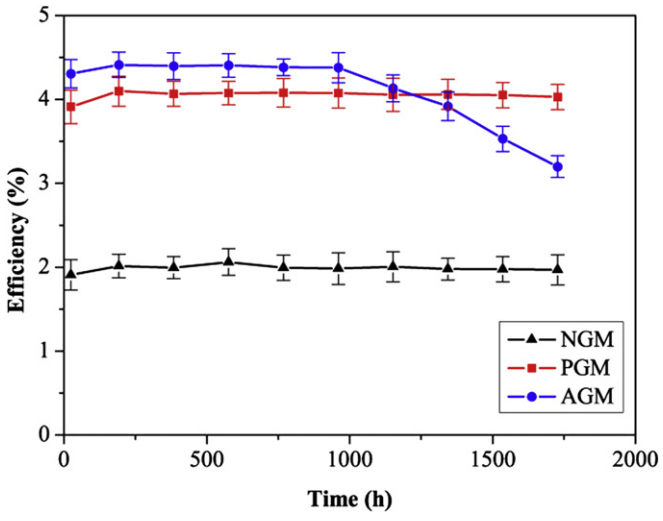

Fig. 9. Performance of the NGM (line with triangle points), PGM (line with square points) and AGM (line with circle points) in long-term stability tests.

4. Conclusion

In this study, an attempt is made to improve the long-term durability of the parallel-grid DSSC module using a Pt metal grid instead of the conventional Ag metal grid. The Pt metal grid is fabricated by DC magnetron sputtering with substrate heat treatment. The R_S of the Pt grid is reduced by increasing the sputter deposition time, until saturation. The minimum R_S of the Pt grid is 1.092 Ω square^{-1} without damaging the grid structure after DC sputter deposition for 15 min with substrate heat treatment at 150 °C. Although the R_S of the Pt grid is slightly higher than that of the Ag grid, the Pt metal is sufficient to act as the electron-collecting grid. As a result, the initial performance of the PGM is better than that of the NGM. After the long-term durability test for 1700 h, the performance of the PGM is maintained as 4.1% AM 1.5 efficiency, whereas the performance of the AGM is <80% of its initial performance, because there is no electrolyte degradation or grid corrosion due to the electrolyte. Therefore, the durability of the PGM is improved owing to its relative inertness to the electrolyte, despite the initial performance being slightly lower than the AGM. Overall, Pt metal is believed to be effective as a grid structure and suitable to a durable parallel-grid DSSC module.

Acknowledgements

This work was supported by National Research Foundation of Korea (NRF) grant funded by the Korea government (MEST) (No. 20110001295).

Appendix A. Supplementary data

Supplementary data related to this article can be found at http://dx.doi.org/10.1016/j.jpowsour.2012.08.080.

References

[1] B. O'Regan, M. Gratzel, Nature 353 (1991) 737–740.
[2] M. Gratzel, Inorg. Chem. 44 (2005) 6841–6851.
[3] S. Cha, Y. Kim, K.H. Hwang, Y.J. Shin, S.H. Seo, D.Y. Lee, Energy Environ. Sci. 5 (2012) 6071–6075.
[4] A. Yella, H.W. Lee, H.N. Tsao, C. Yi, A.K. Chandiran, Md.K. Nazeeruddin, E.W.G. Diau, C.Y. Yeh, S.M. Zakeeruddin, M. Gratzel, Science 334 (2011) 629–633.
[5] M.A. Green, K. Emery, Y. Hishikawa, W. Warta, E.D. Dunlop, Prog. Photovolt.: Res. Appl. 20 (2012) 12–20.

[6] C.P. Lee, M.H. Yeh, R. Vittal, K.C. Ho, J. Mater. Chem. 21 (2011) 15471–15478.
[7] G. Wang, S. Zhuo, L. Wang, S. Fang, Y. Lin, Sol. Energy 86 (2012) 1546–1551.
[8] Q. Yu, C. Yu, F. Guo, J. Wang, S. Jiao, S. Gao, H. Li, L. Zhao, Energy Environ. Sci. 5 (2012) 6151–6155.
[9] F. Ribeiro, J. Macaira, R. Cruz, J. Gabriel, L. Andrade, A. Mendes, Sol. Energy Mater. Sol. Cells 96 (2012) 43–49.
[10] R. Sastrawan, J. Beier, U. Belledin, S. Hemming, A. Hinsch, R. Kern, C. Vetter, F.M. Petrat, A. Prodi-Schwab, P. Lechner, W. Hoffmann, Sol. Energy Mater. Sol. Cells 90 (2006) 1680–1691.
[11] T. Kitamura, K. Okada, H. Matsui, N. Tanabe, J. Sol. Energy-T ASME 132 (2010) 021105.
[12] J.L. Lan, C.C. Wan, T.C. Wei, W.C. Hsu, Y.H. Chang, Prog. Photovolt.: Res. Appl. 20 (2012) 44–50.
[13] J.H. Yum, S.J. Moon, C.S. Karthikeyan, H. Wietasch, M. Thelakkat, S.M. Zakeeruddin, Md.K. Nazeeruddin, M. Gratzel, Nano Energy 1 (2012) 6–12.
[14] N. Kato, K. Higuchi, H. Tanaka, J. Nakajima, T. Sano, T. Toyoda, Sol. Energy Mater. Sol. Cells 95 (2011) 301–305.
[15] L. Han, A. Fukui, Y. Chiba, A. Islam, R. Komiya, N. Fuke, N. Koide, R. Yamanaka, M. Shimizu, Appl. Phys. Lett. 94 (2009) 013305.
[16] H. Seo, M. Son, J. Hong, D.Y. Lee, T.P. An, H. Kim, H.J. Kim, Sol. Energy 83 (2009) 2217–2222.
[17] Y. Takeda, N. Kato, K. Higuchi, A. Takeichi, T. Motohiro, S. Fukumoto, T. Sano, T. Toyoda, Sol. Energy Mater. Sol. Cells 93 (2009) 808–811.
[18] S. Dai, J. Weng, Y. Sui, C. Shi, Y. Huang, S. Chen, X. Pan, X. Fang, L. Hu, F. Kong, K. Wang, Sol. Energy Mater. Sol. Cells 84 (2004) 125–133.
[19] E. Ramasamy, W.J. Lee, D.Y. Lee, J.S. Song, J. Power Sources 165 (2007) 446–449.
[20] W.J. Lee, E. Ramasamy, D.Y. Lee, J.S. Song, Sol. Energy Mater. Sol. Cells 91 (2007) 1676–1680.
[21] S. Dai, J. Weng, Y. Sui, S. Chen, S. Xiao, Y. Huang, F. Kong, X. Pan, L. Hu, C. Zhang, K. Wang, Inorg. Chim. Acta 361 (2008) 786–791.
[22] S.H. Seo, H.J. Kim, B.K. Koo, D.Y. Lee, J. Electrochem. Soc. 156 (2009) F128–F130.
[23] G.E. Tulloch, J. Photochem. Photobiol. A 164 (2004) 209–219.
[24] L. Wang, X. Fang, Z. Zhang, Renew. Sust. Energ. Rev. 14 (2010) 3178–3184.
[25] H. Matsui, K. Okada, T. Kitamura, N. Tanabe, Sol. Energy Mater. Sol. Cells 93 (2009) 1110–1115.
[26] M. Ikegami, J. Suzuki, K. Teshima, M. Kawaraya, T. Miyasaka, Sol. Energy Mater. Sol. Cells 93 (2009) 836–839.
[27] L. Morales, B. Andreosso-O'Callaghan, Res. Int. Bus. Finance 25 (2011) 203–227.
[28] J.M. Kroon, N.J. Bakker, H.J.P. Smit, P. Liska, K.R. Thampi, P. Wang, S.M. Zakeeruddin, M. Gratzel, A. Hinsch, S. Hore, U. Wurfel, R. Sastrawan, J.R. Durrant, E. Palomares, H. Pattersson, T. Gruszecki, J. Walter, K. Skupien, G.E. Tulloch, Prog. Photovolt.: Res. Appl. 15 (2007) 1–18.
[29] K. Park, D. Seo, J. Lee, Colloids Surf. A 313–314 (2008) 351–354.
[30] J.H. Sohn, L.Q. Pham, H.S. Kang, J.H. Park, B.C. Lee, Y.S. Kang, Radiat. Phys. Chem. 79 (2010) 1149–1153.
[31] Y. Huang, S. Dai, S. Chen, C. Zhang, Y. Sui, S. Xiao, L. Hu, Appl. Phys. Lett. 95 (2009) 243503.
[32] R.A. Serway, Principles of Physics, second ed. Forth Worth, Texas, London, 1998.
[33] N. Koide, A. Islam, Y. Chiba, L. Han, J. Photochem. Photobiol. A 182 (2006) 296–305.
[34] F. Fabregat-Santiago, J. Bisquert, G. Garcia-Belmonte, G. Boschloo, A. Hagfeldt, Sol. Energy Mater. Sol. Cells 87 (2005) 117–131.
[35] F. Fabregat-Santiago, J. Bisquert, E. Palomares, L. Otero, D. Kuang, S.M. Zakeeruddin, M. Gratzel, J. Phys. Chem. C 111 (2007) 6550–6560.
[36] Q. Wang, S. Ito, M. Gratzel, F. Fabregat-Santiago, I. Mora-Sero, J. Bisquert, T. Bessho, H. Imai, J. Phys. Chem. B 110 (2006) 25210–25221.
[37] Y. Tachibana, K. Hara, K. Sayama, H. Arakawa, Chem. Mater. 14 (2002) 2527–2535.
[38] J.S. Salafsky, W.H. Lubberhuizen, E. Van Faassen, R.E.I. Schropp, J. Phys. Chem. B 102 (1998) 766–769.